Journal of Photochemistry and Photobiology 33 (2026) 100286

Contents lists available at ScienceDirect

Journal of Photochemistry and Photobiology

journal homepage: www.sciencedirect.com/journal/journal-of-photochemistry-and-photobiology

Polychromatic photobiomodulation accelerates diabetic wound repair via pro-angiogenic and anti-inflammatory mechanisms

Burcu Sarıkaya [a], Furkan Batuhan Çetin [b], Gülnur Take Kaplanoğlu [b], Menemşe Gümüşderelioğlu [c,*]

[a] Balıkesir University, Faculty of Medicine, Department of Medical Genetics, Balıkesir, Turkey
[b] Gazi University, Faculty of Medicine, Department of Histology and Embryology, Ankara, Turkey
[c] Hacettepe University, Graduate School of Science and Engineering, Bioengineering Division, Ankara, Turkey

ARTICLE INFO

Keywords:
Diabetic foot ulcer
Wound healing
Photobiomodulation
Polychromatic light
In vivo

ABSTRACT

This study aimed to evaluate the histological and molecular effects of polychromatic photobiomodulation (PBM, 600–1200 nm), delivered at varying treatment frequencies, on wound healing in a streptozotocin (STZ)-induced diabetic rat model. To minimize inter-subject variability, three full-thickness excisional wounds were created on the dorsum of each diabetic rat and assigned to one of three groups: untreated Negative Control (NC), once-daily PBM (PBM1), or twice-daily PBM (PBM2). Treatments were administered using a polychromatic light source (600–1200 nm) placed 30 cm away from the wounds at an irradiance of 0.038 W/cm^2 with escalating fluences over a six-day period. Skin samples were harvested on Days 7 and 14 post-wounding and analyzed using Masson's Trichrome staining and immunohistochemistry for VEGF, VEGFR2, TGF-β, TGF-βR2, CD163, and TNF-α. The PBM2 regimen significantly enhanced re-epithelialization, collagen deposition, and angiogenesis compared to both PBM1 and untreated controls. Immunohistochemical analysis demonstrated early and pronounced expression of VEGF and CD163, along with sustained activation of TGF-βR2 in the PBM2 group. TNF-α expression was significantly reduced, particularly in the PBM2-treated wounds, suggesting accelerated resolution of inflammation and enhanced M2 macrophage polarization. Masson's Trichrome staining further confirmed the presence of denser and more organized collagen fibers in PBM2-treated wounds. Collectively, these findings indicate that twice-daily polychromatic PBM facilitates diabetic wound healing through synergistic pro-angiogenic, anti-inflammatory, and fibroproliferative pathways. This study supports the further optimization of PBM protocols for the effective management of chronic wounds.

Abbreviations

AdMSC	Adipose-derived mesenchymal stem cell
α-SMA	Alpha-smooth muscle actin
CCO	Cytochrome c oxidase
CD163	Cluster of differentiation 163 (M2 macrophage marker)
cAMP	Cyclic adenosine monophosphate
COX-2	Cyclooxygenase-2
DAB	3,3′-Diaminobenzidine
DFU / DFUs	Diabetic foot ulcer(s)
ECM	Extracellular matrix
EGF	Epidermal growth factor
FGF	Fibroblast growth factor
HDF	Human dermal fibroblast
HIF-1α	Hypoxia-inducible factor 1-alpha
HS2	Human keratinocyte cell line (HS2)
HUVEC	Human umbilical vein endothelial cell
IHC	Immunohistochemistry
IL-1β / IL-6	Interleukin-1 beta / Interleukin-6
LLLT	Low-level laser therapy
MAPK / JNK	Mitogen-activated protein kinase / c-Jun N-terminal kinase
NC	Negative control
NF?B	Nuclear factor kappa B
NO	Nitric oxide
NPWT	Negative pressure wound therapy

* Corresponding author at: Graduate School of Science and Engineering, Hacettepe University, 06800, Ankara, Turkey.
E-mail addresses: brcsarikaya@gmail.com (B. Sarıkaya), furkanbatuhancetin1997@hotmail.com (F. Batuhan Çetin), gulnurtake@gmail.com (G.T. Kaplanoğlu), menemse@gmail.com (M. Gümüşderelioğlu).

https://doi.org/10.1016/j.jpap.2026.100286

Available online 13 April 2026

PAD	Peripheral arterial disease
PBM	Photobiomodulation
PBM1 / PBM2	Once-daily / twice-daily photobiomodulation
PDGF	Platelet-derived growth factor
ROS	Reactive oxygen species
STZ	Streptozotocin
TGF-ß	Transforming growth factor-beta
TGF-ßR2	Transforming growth factor-beta receptor 2
TNF-a	Tumor necrosis factor-alpha
TRPV	Transient receptor potential vanilloid
VEGF	Vascular endothelial growth factor
VEGFR2	Vascular endothelial growth factor receptor 2
VSMC	Vascular smooth muscle cell

1. Introduction

Diabetes-associated foot ulcer (DFU) is a severe complication affecting approximately 19–34% of diabetic individuals, frequently leading to lower limb amputation and significant mortality [1–3]. Current clinical management strategies are multimodal, encompassing debridement, infection control with antibiotics, off-loading devices, and advanced wound dressings such as bioengineered matrices, skin substitutes, and negative pressure wound therapy (NPWT) [4–7]. Despite these extensive therapeutic options, healing outcomes remain frequently suboptimal due to the complex impaired physiological environment of diabetic wounds [8], necessitating the development of novel adjunctive therapeutic modalities.

Photobiomodulation (PBM), formerly known as low-level laser therapy (LLLT), is a therapeutic approach based on exposing tissues to non-ionizing, low-intensity red (600–700 nm) to near-infrared (700–1400 nm) light. After absorption by endogenous chromophores, it triggers a cascade of biological responses [9]. Tina Karu first demonstrated that red and near-infrared light are absorbed by mitochondrial cytochrome c oxidase in the electron transport chain [10]. Unlike thermal therapies, PBM acts via photochemical mechanisms mediated mainly by cytochrome c oxidase (CCO) and transient receptor potential vanilloid (TRPV) channels. In the 600–810 nm range, CCO activation enhances mitochondrial respiration, inducing a mild, transient increase in Reactive Oxygen Species (ROS) that functions as a beneficial secondary signaling pathway rather than causing oxidative stress [11,12]. This process also increases nitric oxide (NO), adenosine triphosphate (ATP), and cyclic adenosine monophosphate (cAMP) production. In the 800–1064 nm range, PBM primarily activates TRPV channels, promoting Ca^{2+} influx and elevating intracellular calcium levels [11].

Moreover, PBM augments NO bioavailability through both direct photolysis and CCO-mediated nitrite reduction, promoting vasodilation, antioxidant defense, analgesia, and cardiovascular function. Secondary messengers such as ROS, NO, cAMP, and Ca^{2+} subsequently activate various transcription factors and intracellular signaling pathways, including the MAPK/JNK cascade, ultimately modulating gene expression and suppressing pro-inflammatory mediators such as TNF-α, IL-1β, IL-6, and COX-2 [13]. Collectively, these molecular events downregulate inflammation and apoptosis while upregulating growth factors including VEGF, EGF, PDGF, FGF, and TGF-β1—thus supporting fibroblast migration, proliferation, and overall tissue regeneration [14].

Numerous studies have investigated PBM in diabetic ulcer treatment, though optimal parameters and mechanisms remain to be fully clarified. Chung et al. [15] evaluated 660 nm at 0, 0.8, 1.6, and 3.2 J/cm^2 in diabetic mice and identified 3.2 J/cm^2 as most effective for reepithelialization and granulation. Santos et al. [16] compared 660 nm and 790 nm in diabetic rats, showing superior flap survival, angiogenesis, and fibroblast proliferation with 790 nm. In a multi-wavelength comparison (532, 633, 810, 980, and 10,600 nm), Al-Watban [17] reported that 633 nm applied three times weekly improved healing by over 40%, nearly restoring normal rates. Hegde et al. [18] found that a single 3 J/cm^2 He–Ne dose immediately post-injury was more effective than multiple doses in enhancing wound contraction and collagen deposition. Güngörmüş and Akyol [19] demonstrated that daily 808 nm at 10 J/cm^2 significantly accelerated inflammation resolution and reepithelialization. Clinically, Pakkiriappan et al. [20] showed that 635 nm irradiation for three weeks resulted in approximately fourfold faster DFU closure compared to controls. Overall, these findings highlight PBM's therapeutic potential in diabetic wound healing and the critical importance of wavelength- and dose-specific protocols for optimizing clinical outcomes.

In the present study, we investigated the therapeutic efficacy of a polychromatic light source (600–1200 nm) on streptozotocin (STZ)-induced diabetic wounds. Unlike previous studies limited to single wavelengths or fixed-dose regimens [15–19], this research addresses a critical knowledge gap regarding the temporal frequency of PBM application. We hypothesize that overcoming the metabolic inertia of diabetic tissue requires sustained, high-frequency stimulation rather than a static dose. Consequently, this study evaluates the ability of a specific dose–frequency protocol to enhance angiogenic (VEGF/-VEGFR2) and fibrogenic (TGF-β/TGF-βR2) pathways while modulating inflammation (CD163) through integrative histological and immunohistochemical analyses.

2. Materials & methods

2.1. Reagents

To induce experimental diabetes, Streptozotocin (STZ) was utilized (Cayman, USA) and sodium citrate was obtained from Sigma-Aldrich (USA). Among the anesthetic agents used in the *in vivo* experiments, ketamine was supplied by Doğa İlaç (Turkey), and xylazine was purchased from IPM (Turkey). The Masson's Trichrome with Aniline Blue kit was obtained from Bio Optica-Milano Spa (Lot: 09211, Italy). For immunohistochemical analyses, the UltraVision Detection System Anti-Polyvalent HRP Kit, DAB Chromogen Kit, and UV Hydrogen Peroxide Block were provided by Thermo Scientific (USA). The primary antibodies used in the study—VEGF (bs-1665R), VEGFR2 (bs-10412R), TNF-α (bs-2081R), CD163 (bs-2527R), TGF-β (bs-0086R), and TGF-βR2 (bs-0117R)—were all purchased from Bioss (USA).

2.2. Establishment of the diabetes model

The flow chart of the applications performed in this study is shown schematically in Fig. 1. Healthy male Wistar albino rats (six weeks old, 190 ± 10 g) were obtained from the Laboratory Animal Breeding and Experimental Research Center of Gazi University (GÜDAM, Turkey). All experimental procedures were approved by the Animal Ethics Committee of Gazi University (Ankara, Turkey) under the protocol number G.Ü.ET-23.046. The animals were housed under controlled conditions at 22 ± 2°C, with 55 ± 10% relative humidity and a 12 h light/dark cycle. They were provided with a standard diet and water ad libitum throughout the study.

To induce diabetes, a total of 20 Wistar albino rats received an intraperitoneal (i.p.) injection of STZ at a dose of 50 mg/kg. STZ was freshly dissolved in a cold 0.1 M sodium citrate buffer (pH 4.5), prepared in the dark. Each rat (weighing between 175 and 200 g) received an average injection volume of 0.5 mL, adjusted based on body weight. Following the injection, the animals continued to be fed ad libitum.

Seven days post-injection, fasting blood glucose levels were measured using a glucometer (Accu-Chek, Roche, Switzerland). Rats with blood glucose levels exceeding 250 mg/dL were considered diabetic. For those that did not meet this threshold, STZ injections were repeated at an increased dose of 65 mg/kg on two additional occasions. As a result, a stable diabetes model was successfully established in 12 rats.

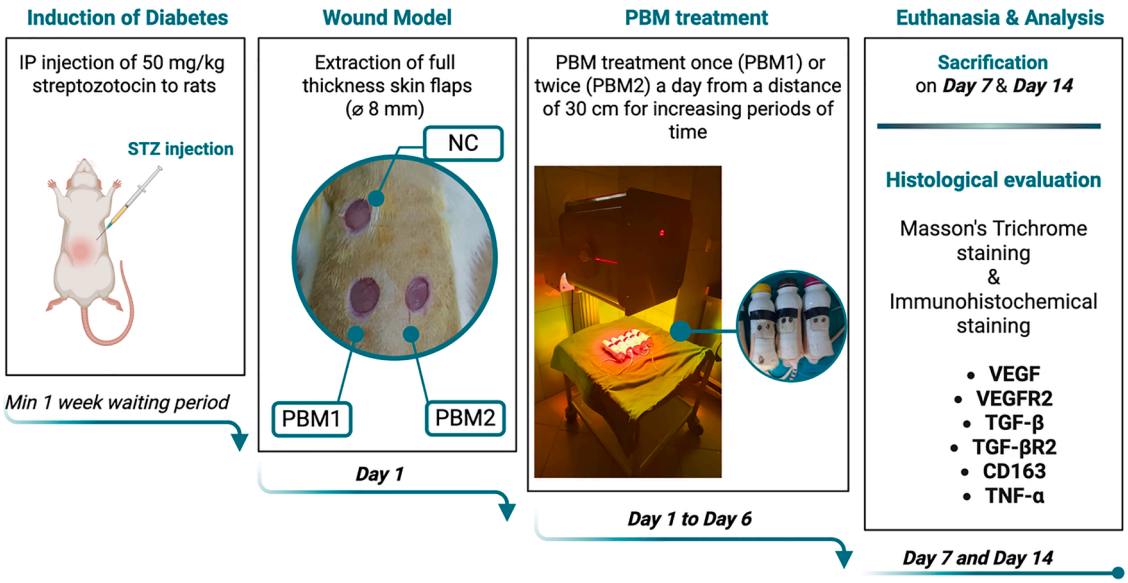

Fig. 1. Experimental workflow illustrating diabetes induction, wound creation, photobiomodulation (PBM) treatment regimen, and subsequent histological evaluation in the STZ induced diabetic rat model.

2.3. In vivo studies

To establish a diabetic ulcer model in rats, animals were anesthetized with ketamine (80 mg/kg) and xylazine (10 mg/kg). The dorsal area was shaved, disinfected with povidone-iodine, and three 8 mm full-thickness wounds were created using a biopsy punch (Premier, India). Wounds were assigned to Negative Control (NC), PBM once daily (PBM1), or PBM twice daily (PBM2). NC received no treatment, PBM1 was treated once daily, and PBM2 twice daily for six days at 30 cm, with exposure duration gradually increased. A split-body design allowed each rat to serve as its own control, minimizing inter-subject variability [21,22].

Rats were immobilized using a custom cylindrical tube with air-permeable holes and a window for direct light exposure, while non-target wounds were shielded with sterile markers and black tape to prevent cross-exposure. For PBM studies, an FDA-approved plasma arc light source (PAC; Collagentex RX-1, Tanses Technologies, Canada) was employed. The device emits light at 10 discrete wavelengths between 600 and 1200 nm, delivering a total energy fluence of 52 J/cm^2 over an exposure area of 1150 cm^2, at a distance of 20 cm, during a 20-minute treatment [23–25]. Irradiation parameters were based on prior LLLT studies, with an irradiance of 0.038 W/cm^2 at a distance of 30 cm from the wound, and escalating fluences applied over a six-day period. Treatment durations were adjusted according to wound healing stages (see Table 1).

2.4. Macroscopic analysis

The therapeutic efficacy of PBM on wound closure was evaluated through direct morphometric assessment. Wound dimensions were recorded at Day 0 and at the specific experimental endpoints (Day 7 and Day 14) immediately prior to sacrifice. Measurements were obtained using a precision metric caliper to ensure accuracy. The macroscopic changes were quantified by calculating the percentage of wound contraction relative to the initial wound size. The wound closure rate (%) was determined using the following standard formula:

$$\text{Wound Closure Rate } (\%) = \frac{(A_i - A_s)}{A_i} \times 100 \quad (1)$$

where A_i represents the initial wound area on Day 0, and A_s represents the wound area measured on the day of sacrifice (Day 7 or Day 14) [21,26,27].

2.5. Histological examination by light microscopy

Rats were randomly assigned to two groups and euthanized on days 7 and 14 post-wounding using high-dose anesthesia. Dorsal skin samples were collected and fixed in 10% neutral buffered formalin for at least 72 h. Samples were rinsed under running water for 24 h, dehydrated through a graded ethanol series (70–100%), cleared in xylene, and embedded in paraffin. Serial 4 μm sections were prepared and stained with Masson's Trichrome or subjected to immunohistochemistry. Histological evaluation and imaging were performed using the Leica DCM4000 system with LAS software (Leica Microsystems, Germany).

2.5.1. Masson's trichrome staining

For deparaffinization, tissue sections were incubated overnight at 37°C, then heated at 57–63°C for 2 h and immersed in xylene twice for 15 min each. Sections were rehydrated through a graded ethanol series (100%, 96%, 80%) for 10 min each and rinsed twice in distilled water.

Masson's Trichrome staining (Aniline Blue kit) was performed by

Table 1
Photobiomodulation (PBM) parameters applied in experimental groups.

	PBM1			PBM2		
	Duration (min)	*Repetition*	*Cumulative dose* (J/cm^2)	*Duration* (min)	*Repetition*	*Cumulative dose* (J/cm^2)
Day 1 & 2	6	Once daily	13.8	6	Twice daily	27.6
Day 3 & 4	11	Once daily	25.3	11	Twice daily	50.6
Day 5 & 6	20	Once daily	46.0	20	Twice daily	92.0
Distance		30 cm			30 cm	

incubating sections in Weigert's iron hematoxylin for 10 min, followed by picric acid–alcohol for 4 min, Ponceau acid fuchsin for 4 min, phosphomolybdic acid for 10 min, and aniline blue for 5 min, with distilled water rinses between steps. Stained sections were dehydrated through ascending alcohols, cleared in xylene, and mounted with Entellan.

2.5.2. Immunohistochemical staining

Tissue sections on poly-L-lysine slides were incubated overnight at 37°C, heated at 60°C for 1 h, and immersed in xylene three times. Sections were rehydrated through graded ethanol (100%, 96%, 80%) and washed in distilled water. Antigen retrieval was performed in 1 M citrate buffer (pH 6.0) in a microwave, followed by cooling. Endogenous peroxidase was blocked with 3% hydrogen peroxide, and sections were rinsed with PBS [20].

Immunohistochemistry used the UltraVision Detection System with primary antibodies (1:200) for VEGF, VEGFR2, TGF-β, TGF-βR2, TNF-α, and CD163, incubated overnight at 4°C. Slides were treated with Biotinylated Goat Anti-Polyvalent and Streptavidin Peroxidase, developed with DAB, counterstained with Harris' hematoxylin, and mounted with Entellan.

2.6. Statistical analysis

All data are presented as mean ± standard deviation (SD) from representative experiments performed in triplicate. Statistical analyses were conducted using GraphPad InStat software. Group differences were assessed using one-way analysis of variance (ANOVA), followed by unpaired Student's ***t***-tests for pairwise comparisons where appropriate. A p-value of <0.05 ($p < 0.05$) was considered statistically significant.

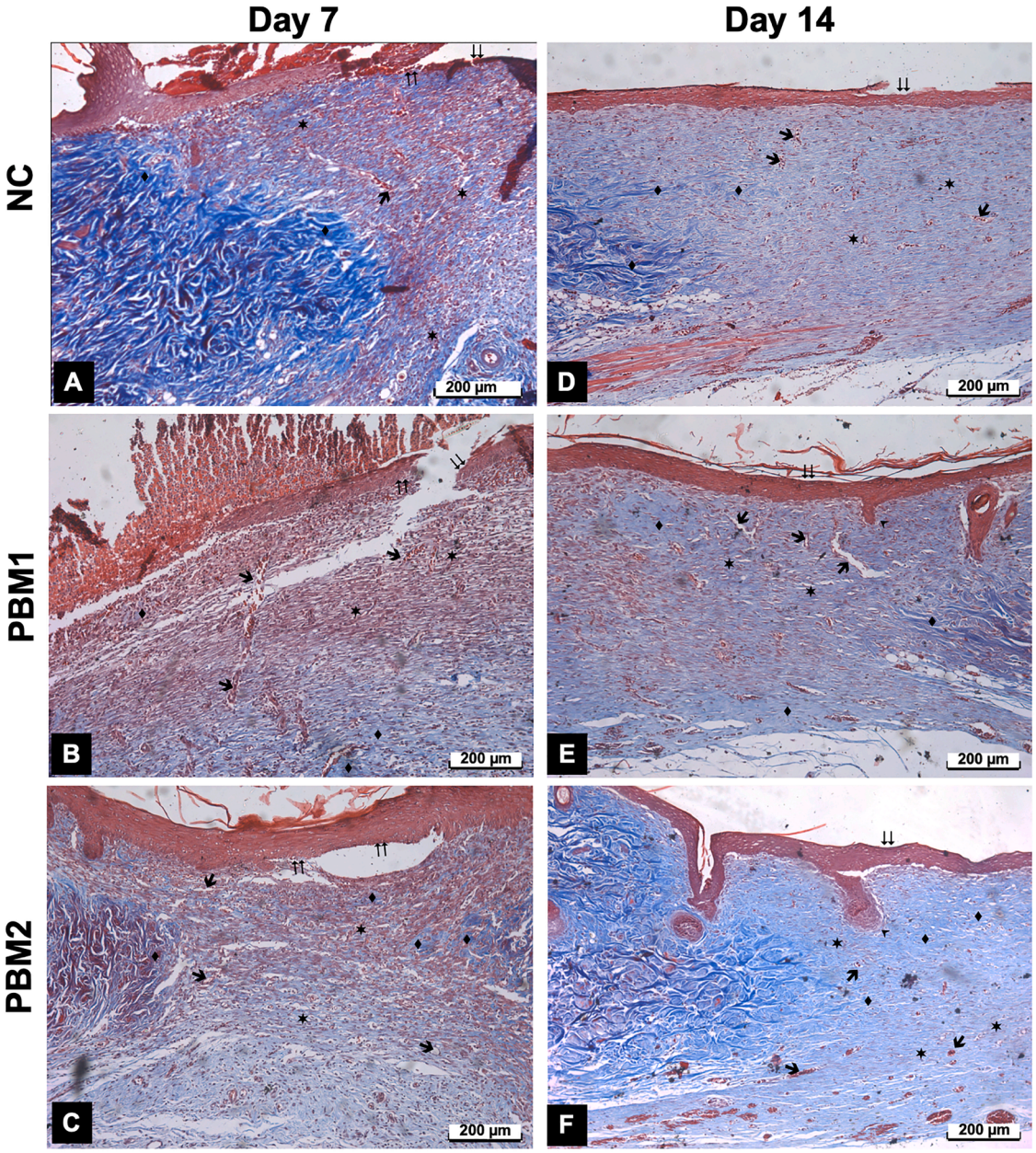

Fig. 2. Masson's trichrome staining. A-C) Day 7, NC group without PBM treatment, PBM1 group receiving PBM once daily, PBM2 group receiving PBM twice daily, respectively. D-F) Day 14, NC group without PBM treatment, PBM1 group receiving PBM once daily, PBM2 group receiving PBM twice daily, respectively. (⇉): wound site epithelium, (✶): wound site dermal connective tissue, (↟): blood vessels, (⧫): normal dermis adjacent to the wound site (Masson's trichrome, X100).

3. Results

3.1. Masson's trichrome staining

Masson's Trichrome staining was used to assess collagen deposition and structural organization in wound tissue. On Day 7, the NC group showed incomplete re-epithelialization and disorganized dermis, with granulation tissue containing thin, lightly stained collagen fibers and high cellularity (Fig. 2A). The PBM1 group exhibited more advanced dermal healing, reduced granulation tissue, early collagen bundles, and increased vascularity (Fig. 2B). PBM2 showed the greatest progression, with a basal epithelial layer forming, bridged wound edges, diminished granulation tissue, and pronounced vascularization, indicating accelerated transition from inflammation to proliferation (Fig. 2C).

By Day 14, epithelialization was macroscopically complete in all groups, but histological maturity differed. NC had immature epithelium and disorganized dermis (Fig. 2D). PBM1 displayed thicker epithelium, early hair follicle formation, and partially organized dermis (Fig. 2E). PBM2 presented fully stratified, keratinized epithelium with dense, parallel collagen bundles and active dermal remodeling, indicating superior tissue maturation (Fig. 2F).

These histological improvements in tissue organization were paralleled by macroscopic observations of wound closure. Although statistical significance was limited by intragroup variability ($p > 0.05$), PBM-treated groups demonstrated a clear trend toward accelerated healing in closure rates compared to the control. On Day 7, the wound closure rate was 59.6 ± 27.6% in the PBM1 group and 58.0 ± 21.3% in the PBM2 group, whereas the NC group exhibited a lower closure rate of 46.0 ± 18.4%. This trend persisted through Day 14, where the PBM2 group achieved the highest closure rate of 77.1 ± 12.3%, followed by PBM1 (75.2 ± 11.1%) and NC (69.6 ± 23.5%). Collectively, while wound area measurements did not reach statistical thresholds, the accelerated trend in PBM groups aligns with the superior re-epithelialization and collagen maturity observed in histological analysis.

3.2. Immunohistochemical staining

3.2.1. VEGF

On Day 7, the NC group showed marked VEGF immunoreactivity in the guiding epithelium, connective tissue cells, and deep dermal blood vessels (Fig. 3A). PBM1 exhibited a similar pattern, but VEGF staining was stronger in the superficial dermis and blood vessels (Fig. 3B). PBM2 displayed the most distinct vascular profile, with a complete basal epithelial layer, reduced granulation tissue, pronounced vascularization, and strong VEGF expression in the guiding epithelium and superficial dermis (Fig. 3C). H-score analysis confirmed significantly higher VEGF levels in both PBM groups versus NC ($p < 0.0001$), with PBM2 showing the peak value (Fig. 6A).

By Day 14, NC showed increased VEGF, mainly in the superficial dermis and partially in the epithelium (Fig. 3D). PBM1 maintained robust VEGF expression in the epidermis and dermal connective tissue (Fig. 3E), consistent with a high H-score ($p < 0.0001$). PBM2 showed intense epidermal VEGF but reduced dermal deposition and lower blood vessel density (Fig. 3F). Quantitative analysis indicated that while VEGF remained high in PBM1, PBM2 experienced a significant decline, reflecting an earlier peak in angiogenic activity and progression toward tissue maturation.

3.2.2. VEGFR2

On Day 7, NC showed VEGFR2 immunoreactivity mainly in granulation tissue at wound margins, with deep dermal vessels positive but little staining within the wound itself (Fig. 3G). PBM1 exhibited weak

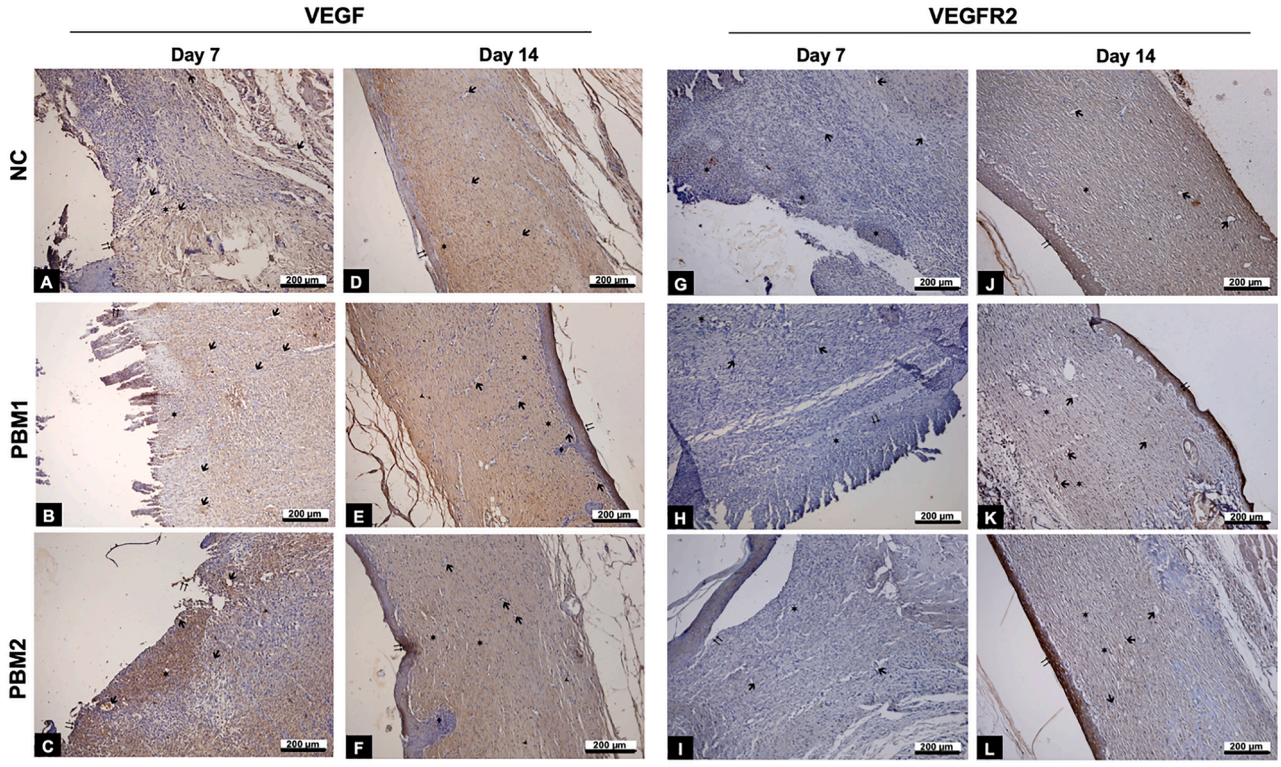

Fig. 3. VEGF and VEGFR2 Immunoreactions. VEGF expression (A–F): A–C) Day 7: NC group without PBM treatment, PBM1 group (once daily), and PBM2 group (twice daily), respectively. D–F) Day 14: NC group, PBM1 group, and PBM2 group, respectively. VEGFR2 expression (G–L): G–I) Day 7: NC group without PBM treatment, PBM1 group (once daily), and PBM2 group (twice daily), respectively. J–L) Day 14: NC group, PBM1 group, and PBM2 group, respectively. (⇉): wound site epithelium, (★): wound site dermal connective tissue, (🡅): deep dermis and surface blood vessels, (⧫): newly formed hair follicles (Immunoperoxidase – Hematoxylin X100).

VEGFR2 in reorganizing dermis, but strong staining in connective tissue of adjacent intact dermis (Fig. 3H). PBM2 showed minimal absent VEGFR2 staining (Fig. 3I). H-score analysis confirmed significantly higher VEGFR2 in PBM1 versus NC and PBM2 ($p < 0.0001$), primarily in intact tissue rather than granulation areas.

By Day 14, NC had VEGFR2 positivity in some deep dermal vessels (Fig. 3J). PBM1 displayed strong staining in deep vessels and surrounding connective tissue (Fig. 3K). PBM2 showed reduced intensity compared to PBM1 but broader spatial distribution across connective tissue and vasculature (Fig. 3L), resulting in the highest H-score among groups ($p < 0.0001$). Temporal analysis indicated peak angiogenic activation occurred earlier in PBM1, while PBM2 induced a delayed yet more extensive response during later healing.

3.2.3. TGF-β

On Day 7, NC showed weak TGF-β in the epidermis near the wound and superficial granulation tissue, with strong staining in the deep dermis (Fig. 4A). PBM1 displayed widespread cytoplasmic staining in fibroblasts and keratinocytes across epidermis and dermis (Fig. 4B), while PBM2 showed elevated but more focal expression in specific dermal structures (Fig. 4C). H-score analysis indicated PBM1 had the highest TGF-β levels, followed by NC and PBM2 ($p < 0.0001$).

By Day 14, NC exhibited moderate epidermal and dermal staining (Fig. 4D). PBM1 showed weak epidermal and moderate superficial/mid-dermal expressions, with a decline in the deep dermis (Fig. 4E). PBM2 demonstrated intense, diffuse TGF-β across epidermis and dermis (Fig. 4F), and H-scores confirmed a significant increase from Day 7, surpassing all other groups ($p < 0.0001$).

3.2.4. TGF-βR2

On Day 7, TGF-βR2 staining was uneven across tissues. NC showed weak to moderate expression mainly in granulation tissue and inflammatory zones (Fig. 4G). PBM1 displayed moderate staining concentrated around basal keratinocytes and dermal fibroblasts (Fig. 4H), while PBM2 exhibited the strongest signal, with intense cytoplasmic staining in fibroblast-like cells and perivascular regions (Fig. 4I). H-score analysis confirmed PBM2 had the highest levels, significantly exceeding PBM1 and NC ($p < 0.0001$).

By Day 14, NC maintained weak to moderate expression in epidermis and dermis (Fig. 4J). PBM1 showed weak to moderate epidermal staining and minimal dermal signal (Fig. 4K). PBM2 retained moderate expression in the superficial dermis, though deep dermal staining declined (Fig. 4L). H-scores indicated that while NC and PBM1 declined over time, PBM2 maintained significantly elevated TGF-βR2 levels ($p < 0.0001$).

3.2.5. CD163

On Day 7, NC showed diffuse CD163 expression in granulation tissue with limited cellular staining (Fig. 5A). PBM1 displayed increased immunoreactivity in superficial and mid-dermis, though still relatively diffuse (Fig. 5B). PBM2 exhibited the strongest, most localized staining, with higher-density CD163-positive M2 macrophages often arranged in organized clusters (Fig. 5C). H-score analysis confirmed PBM2 had the highest expression, significantly exceeding PBM1 and NC ($p < 0.0001$).

By Day 14, all groups shifted to a cell-specific pattern. NC macrophages were mainly in mid- and deep dermis, with epidermal Langerhans cells also positive (Fig. 5D). PBM1 macrophages localized to intact dermis near the wound, with persistent Langerhans cell staining (Fig. 5E). PBM2 showed a similar distribution, but dermal macrophages in the wound area were enlarged, with continued epidermal expression (Fig. 5F). H-scores indicated NC increased modestly over time, while PBM groups maintained significantly elevated levels versus controls ($p < 0.0001$).

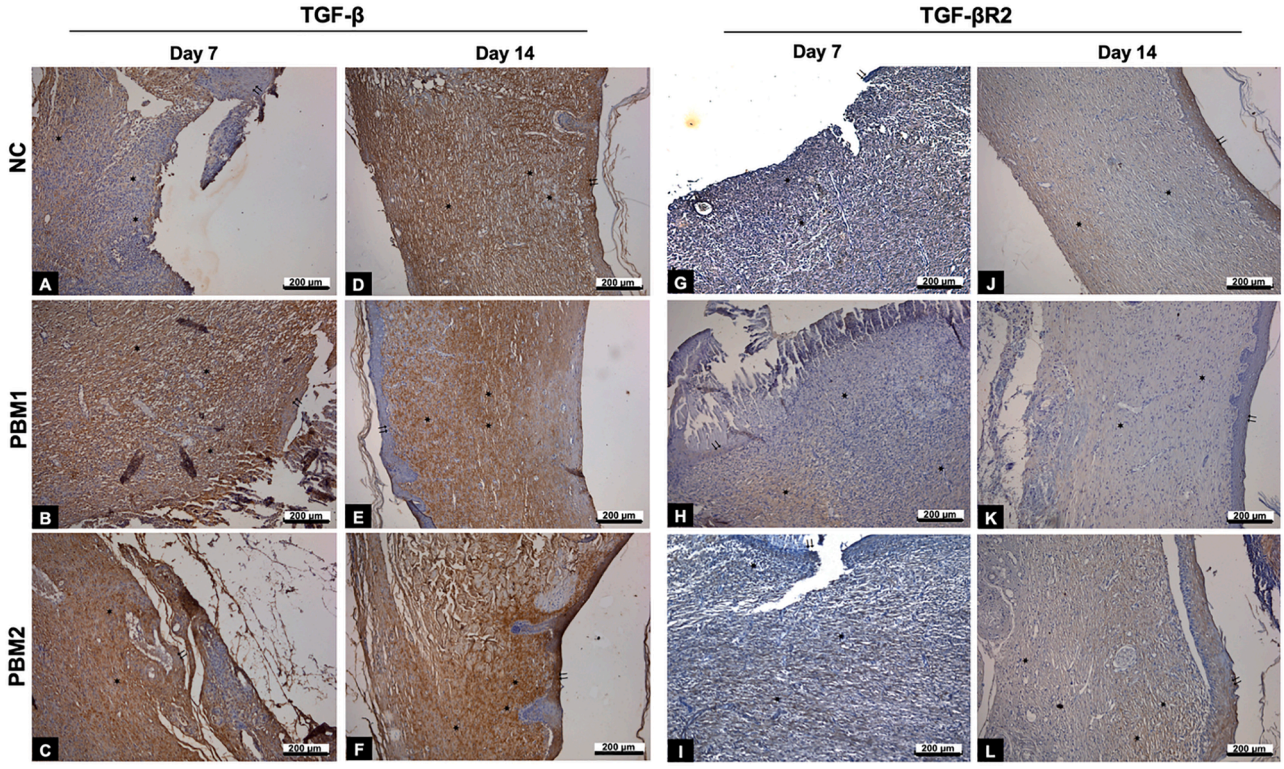

Fig. 4. TGF-β and TGF-βR2 Immunoreactions. TGF-β expression (A–F): A–C) Day 7: NC group without PBM treatment, PBM1 group (once daily), and PBM2 group (twice daily), respectively. D–F) Day 14: NC group, PBM1 group, and PBM2 group, respectively. TGF-βR2 expression (G–L): G–I) Day 7: NC group without PBM treatment, PBM1 group (once daily), and PBM2 group (twice daily), respectively. J–L) Day 14: NC group, PBM1 group, and PBM2 group, respectively. (⇉): wound site epithelium, (⋆): wound site dermal connective tissue, (↑): deep dermis and surface blood vessels. (Immunoperoxidase – Hematoxylin X100).

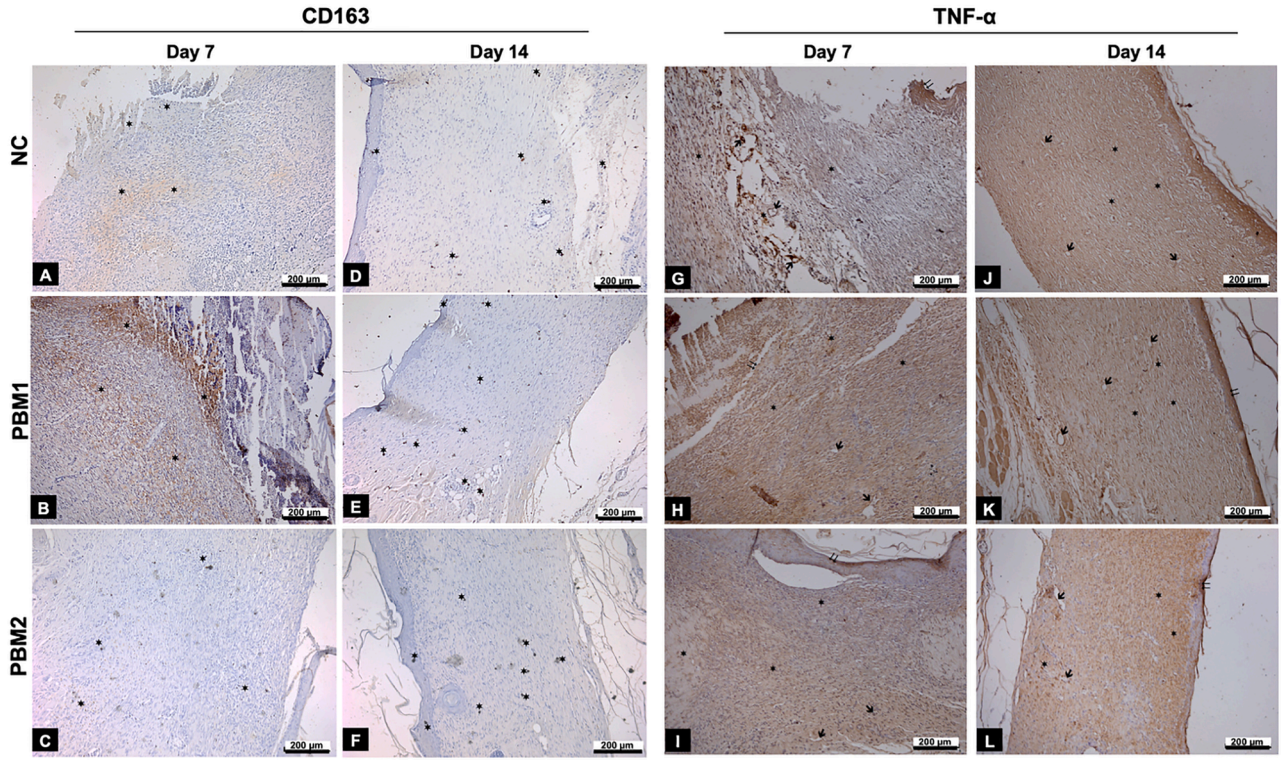

Fig. 5. CD163 and TNF-α Immunoreactions. CD163 expression (A–F): A–C) Day 7: NC group without PBM treatment, PBM1 group (once daily), and PBM2 group (twice daily), respectively. D–F) Day 14: NC group, PBM1 group, and PBM2 group, respectively. TNF-α expression (G–L): G–I) Day 7: NC group without PBM treatment, PBM1 group (once daily), and PBM2 group (twice daily), respectively. J–L) Day 14: NC group, PBM1 group, and PBM2 group, respectively. (⇉): wound site epithelium, (⋆): wound site dermal connective tissue, (🡅): deep dermis and surface blood vessels. (Immunoperoxidase – Haematoxylin X100).

3.2.6. TNF-α

On Day 7, NC showed strong TNF-α expression in the epidermis near the wound, superficial and deep dermis, and in deep dermal blood vessel walls (Fig. 5G). PBM1 displayed less intense but more widespread staining in the guiding epithelium and superficial dermis, with weaker vascular wall deposition (Fig. 5H). PBM2 exhibited weak epidermal but strong diffuse dermal staining, with minimal vascular wall reactivity (Fig. 5I). H-scores confirmed NC had the highest levels, while PBM groups were significantly lower ($p < 0.0001$).

By Day 14, NC and PBM1 maintained strong epidermal and dermal expression, including vascular walls (Fig. 5J, K). PBM2 showed markedly reduced epidermal TNF-α in the fully reorganized epidermis, though dermal expression remained strong, with weak vascular staining (Fig. 5L). H-scores indicated TNF-α remained elevated in NC and PBM1, whereas PBM2 had the lowest levels ($p < 0.0001$).

A comprehensive summary of the histological and immunohistochemical findings, examined across experimental groups and time points (Day 7 and Day 14), is presented in Fig. 7. This integrative overview highlights the accelerated tissue maturation, enhanced angiogenic response, and effective modulation of inflammation observed particularly in the PBM2 group throughout the healing process.

4. Discussion

This study evaluated the therapeutic effects of polychromatic PBM (600–1200 nm) at different doses and frequencies on wound healing in streptozotocin-induced diabetic rats. Twice-daily PBM (PBM2) significantly enhanced angiogenesis, fibrotic signaling, macrophage polarization, and reduced pro-inflammatory cytokines compared to once-daily PBM (PBM1) and controls. These effects were associated with activation of VEGF/VEGFR2 and TGFβ/TGFβR2 pathways, modulation of TNFα and CD163, and improved mitochondrial redox balance [28].

VEGF is a key angiogenic mediator in PBM-induced diabetic wound healing, acting mainly through VEGFR2 to promote angiogenesis, while VEGFR1 is linked to inflammation [28]. On Day 7, VEGF levels increased in both PBM groups, with significantly higher expression in PBM2 [29]. Previous studies support these findings. Zhao et al. showed that 630 nm and 810 nm LED PBM increased VEGF in fibroblasts and elevated VEGF and TGF-β in diabetic mice [29]. In diabetic rats, a 904 nm laser promoted collagen formation, while an 850 nm LED reduced inflammation and enhanced angiogenesis [30]. A 670 nm GaAlAs laser reduced TNF-α and increased VEGF and collagen expression in diabetic wounds [31]. Additionally, Zhang et al. demonstrated that 632 nm PBM activated a VEGFA/VEGFR2/STAT3 positive feedback loop in endothelial cells [32]. These data may explain the temporal differences in VEGF and VEGFR2 responses observed in our study. Sustained VEGFR2 expression under PBM2 suggests prolonged endothelial activation extending into the remodeling phase of wound healing [33].

TGF-β isoforms and their signaling pathways are crucial in all phases of diabetic wound healing, acting through serine/threonine kinase receptors, with TGF-βR2 central to epithelialization, angiogenesis, and ECM synthesis [34]. In this study, TGF-β rose early in PBM1 and controls, but PBM2 showed a delayed increase, reflecting prolonged remodeling. TGF-βR2 expression was significantly higher in PBM2 at both time points, indicating sustained receptor-mediated signaling with more frequent PBM. Supporting studies show similar trends: a 660 nm AlGaInP laser with IL-1Ra reduced inflammation and increased TGF-β and collagen in diabetic rats [35]. Dual-wavelength PBM (660 nm + 808 nm, 2 J/cm^2) also elevated TGF-β by day 10 [36]. Dang et al. reported enhanced TGF-β and Smad2/3/4 expression with 800 nm PBM in non-diabetic rats, though outcomes vary by tissue [37]. In WS1 cells under diabetic/hypoxic conditions, 830 nm PBM increased TGF-β, migration, and proliferation independently of Smad2/3, suggesting effects beyond direct TGF-βR2 activation [38]. Low TGF-βR2 H-scores in

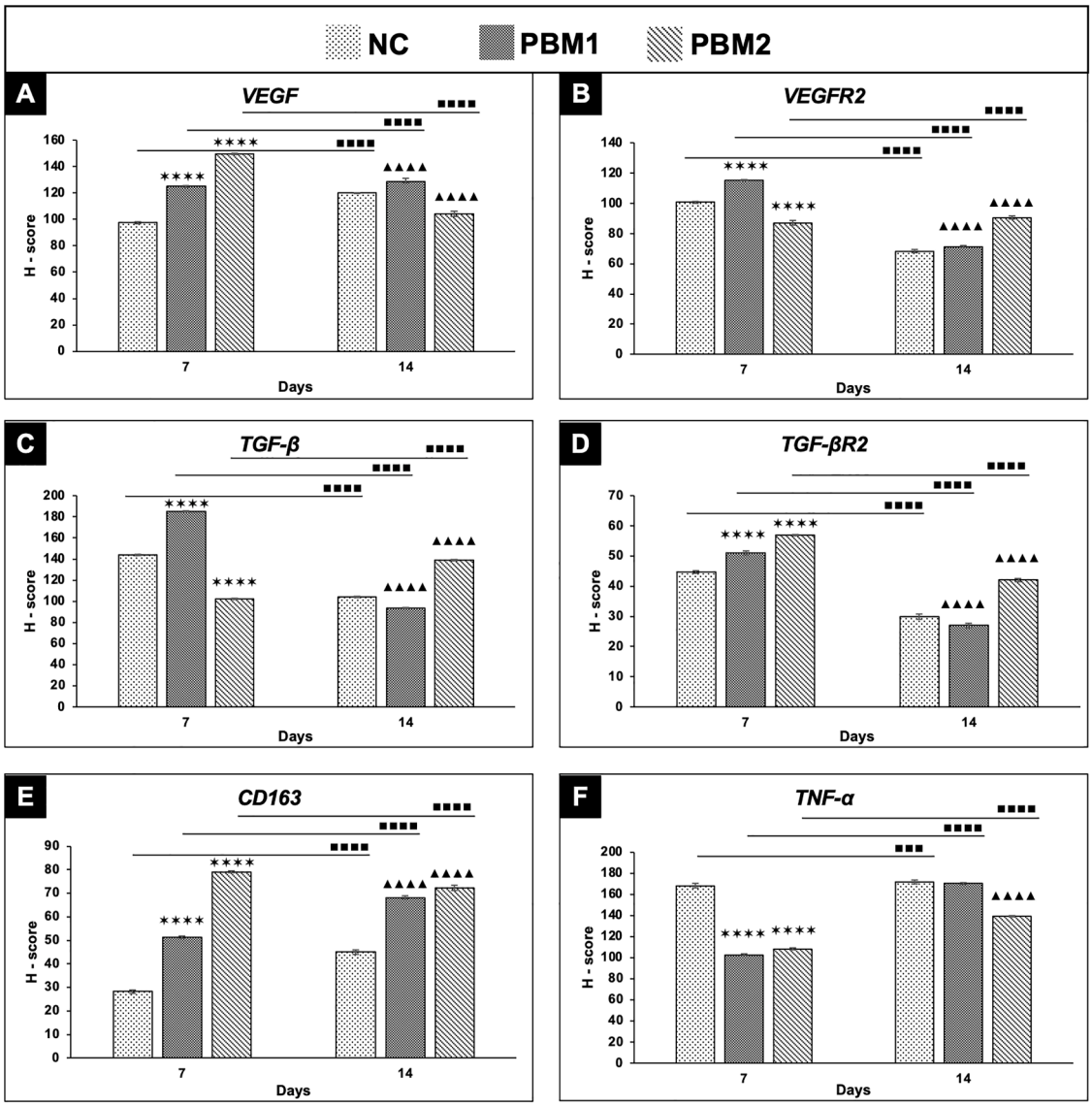

Fig. 6. H-score values in NC, PBM1, and PBM2 groups by IHC for A) VEGF, B) VEGFR2, C) TGF-β, D) TGF-βR2, E) CD163, and F) TNF-α on the 7th and 14th days. The graphs are represented as the mean ±SD (n = 6). Statistically significant differences are denoted by symbols; ****$p < 0.0001$ when compared to the NC group on day 7, ▲▲▲▲$p < 0.0001$ when compared to the NC group on day 14, ■■■■$p < 0.001$, and ■■■■$p < 0.0001$ when compared to the groups between 7th and 14th days.

all groups align with prior reports of chronic wounds, where reduced receptor expression impairs Smad2/3 signaling and hinders tissue regeneration [39,40].

In acute wound healing, M1 pro-inflammatory macrophages clear debris and sustain inflammation, while the M1-to-M2 transition promotes fibroblast activity, cytokine signaling, and dermal/epidermal regeneration. In diabetes, this shift is impaired, prolonging inflammation and contributing to chronic wounds [22]. In our study, TNF-α marked M1 polarization and CD163 indicated M2 polarization. PBM significantly reduced TNF-α, most prominently in PBM2 at Days 7 and 14, while CD163-positive macrophages increased, reflecting enhanced M2 polarization with frequent PBM [41]. Supporting evidence shows that PBM (890 nm, 80 Hz, 3.46 J/cm^2) combined with adipose-derived MSCs boosts M2 polarization, granulation tissue formation, and HIF-1α, VEGF, and FGF expression in diabetic rats [42,43]. Similarly, 830 nm PBM in WS1 fibroblasts under hyperglycemia inhibited NF-κB and reduced TNF-α [44]. TNF-α levels in PBM1 and control wounds were similar on Day 14, consistent with wound-type-dependent PBM effects. Comparative studies indicate PBM can suppress TNF-α in infected or normal wounds but maintain or elevate it in diabetic wounds over 14 days, reflecting a biphasic response [45].

Masson's Trichrome staining revealed denser, more organized collagen in PBM-treated wounds, especially PBM2, with thicker, aligned bundles indicative of advanced remodeling. These results align with Carvalho et al., where 632.8 nm PBM increased collagen content in diabetic and non-diabetic wounds [46]. Mechanistically, the collagen observed in PBM2-treated wounds is consistent with type I collagen fibers, which are essential for restoring tensile strength and structural integrity to the healing tissue. Previous studies have similarly demonstrated that PBM at 660 nm enhances collagen distribution, packing, and alignment by Day 7 in murine models of cutaneous repair and is accompanied by increased recruitment of α-smooth muscle actin (α-SMA)-positive myofibroblasts, facilitating wound contraction and matrix stabilization [47].

The temporal pattern observed—early increases in granulation tissue and collagen deposition, particularly in PBM2—aligns with literature showing that red and near-infrared PBM accelerates fibroblast activation and ECM formation. For example, Reddy et al. reported a 14% increase in collagen content with 904 nm PBM in diabetic rat wounds [48], and Maiya et al. observed complete wound closure by Day 18 with 632.8 nm

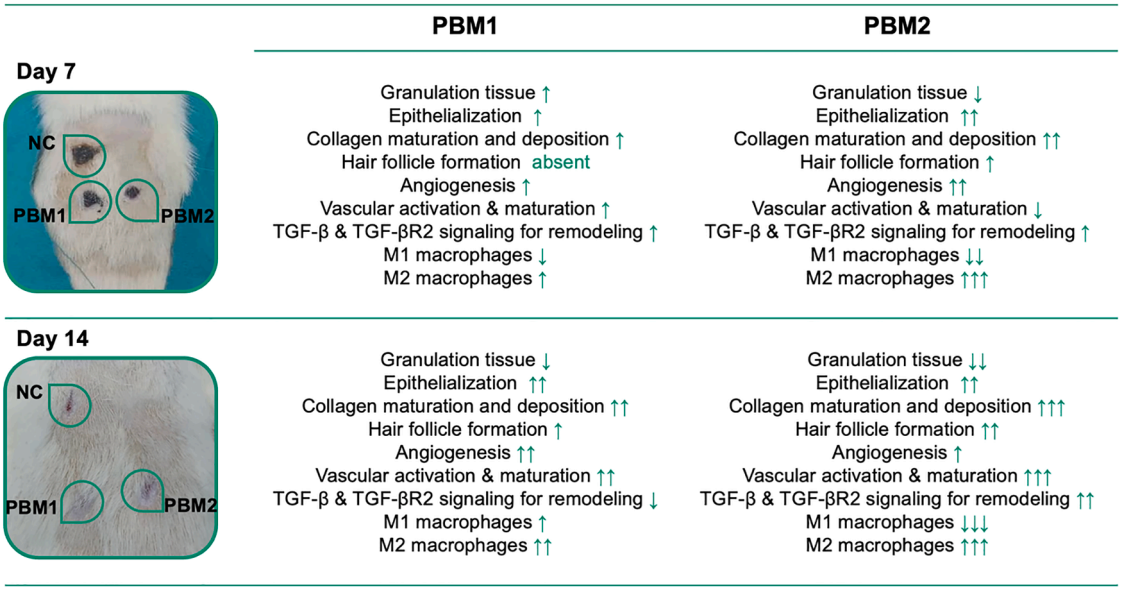

Fig. 7. Comparative summary of histological and immunohistochemical findings in PBM1 and PBM2 groups on Day 7 and Day 14.

PBM, compared to Day 59 in controls, along with thicker collagenous scars [49]. Using the CollagenTex device, PBM enhanced proliferation, migration, and ECM synthesis of HDFs, keratinocytes, and HUVECs under hyperglycemia, notably increasing collagen and fibronectin synthesis and promoting endothelial tube formation [24].

These results indicate that PBM, particularly at optimal fluence and frequency, improves type I collagen fiber synthesis, alignment, and density. This is supported by our immunohistochemistry showing elevated TGF-β and TGF-βR2 under PBM2, linking PBM to fibroblast differentiation and ECM remodeling. Trichrome staining provides both structural and mechanistic evidence of PBM's therapeutic efficacy.

Reviews by Zein et al. and Mgwenya et al. highlight that PBM efficacy depends on mitochondrial density, energy dose, and power density, with most in vivo diabetic wound studies using <100 mW/cm^2 and <5 J/cm^2, applied shortly after wound induction [50–52]. Optimal dosing also depends on wound stage: as healing progresses, increased myofibroblasts and mitochondrial density require higher energy doses to maintain efficacy [50].

Supporting staged dosing, Chung et al. found that 1.6 J/day (3.7–5 J/cm^2) of 660 nm PBM was most effective for diabetic wound repair [15], while Hegde et al. reported that a 3 J/cm^2 632.8 nm dose immediately after wounding accelerated closure [18]. Collectively, these studies underscore the need to tailor PBM parameters—wavelength, energy, power, and frequency—to wound stage and tissue metabolic state, as reflected in our staged, frequency-based PBM regimen.

The PBM protocol delivered polychromatic light at total energy doses of ~14–92 J/cm^2, exceeding conventional ranges of 1–10 J/cm^2 [12,14,52]. However, the broad-spectrum CollagenTex source (633, 666, 712, 812, 1018, 1128 nm) can engage multiple photoreceptors, including cytochrome c oxidase (red wavelengths) and TRPV channels (NIR wavelengths), eliciting diverse biological responses [11]. This multimodal activation may enhance therapeutic effects in complex diabetic wounds.

Although PBM dosing is well-studied, timing and frequency remain underexplored. The superior efficacy of PBM2 over PBM1 aligns with the Arndt-Schultz law, where moderate stimuli enhance activity while excessive doses inhibit it [11,50]. Fractionating the total energy into two daily sessions likely sustained mitochondrial stimulation without inducing inhibitory effects. PBM2 led to earlier VEGF upregulation and prolonged VEGFR2 and TGF-βR2 activation, promoting angiogenesis and tissue remodeling while avoiding excessive fibrosis [11,50].

Limitations include lack of transcriptional or translational confirmation of pathway activation (qPCR, Western blot), absence of functional measures such as mitochondrial redox status and biomechanical tissue strength, and potential systemic effects due to the split-body design. Nevertheless, significant local differences suggest predominant site-specific effects. Future studies should address these gaps to fully elucidate PBM's mechanisms.

5. Conclusion

This study aimed to evaluate the therapeutic efficacy of PBM using a polychromatic light source in a diabetic ulcer model. Given the limited effectiveness of conventional treatments in fully restoring tissue regeneration in diabetic wounds, the primary objective was to stimulate impaired signaling pathways within the wound microenvironment through targeted PBM application. To this end, once-daily and twice-daily PBM protocols, employing progressively increasing irradiation durations, were administered to streptozotocin-induced diabetic ulcers in rats.

In conclusion, twice-daily polychromatic PBM (600–1200 nm) significantly accelerates diabetic wound healing by enhancing angiogenic, fibrotic, antioxidative, and anti-inflammatory pathways. Mechanistically, this involves coordinated upregulation of VEGF/VEGFR2 and TGF-β/TGF-βR2, suppression of TNF-α, and promotion of CD163-positive M2 macrophage polarization. These findings support optimized twice-daily PBM protocol represents a promising, non-invasive adjunctive strategy for the management of chronic, non-healing diabetic ulcers in clinical settings. Future studies should focus on validating these optimized parameters in human clinical trials to establish standardized guidelines.

CRediT authorship contribution statement

Burcu Sarıkaya: Conceptualization, Data curation, Formal analysis, Funding acquisition, Investigation, Methodology, Project administration, Writing – original draft. **Furkan Batuhan Çetin:** Formal analysis, Validation, Visualization. **Gülnur Take Kaplanoğlu:** Investigation, Methodology, Resources, Validation, Visualization. **Menemşe Gümüşderelioğlu:** Conceptualization, Methodology, Supervision, Validation, Writing – review & editing.

Declaration of competing interest

The authors declare that they have no known competing financial interests or personal relationships that could have appeared to influence the work reported in this paper.

Acknowledgement

The authors would like to thank the Gazi University Laboratory Animal Breeding and Experimental Research Center (GUDAM) for their assistance with the animal experiments. This study was financially supported by the Scientific and Technological Research Council of Turkey (TÜBİTAK) under Project No. 2218-122C108.

Data availability

Data will be made available on request.

References

[1] W. Jeffcoate, E.J. Boyko, F. Game, P. Cowled, E. Senneville, R. Fitridge, Causes, prevention, and management of diabetes-related foot ulcers, Lancet Diabetes. Endocrinol. 12 (2024) 472–482, https://doi.org/10.1016/S2213-8587(24)00110-4.
[2] K. McDermott, M. Fang, A.J. Boulton, E. Selvin, C.W. Hicks, Etiology, epidemiology, and disparities in the burden of diabetic foot ulcers, Diabetes Care 46 (1) (2023) 209–221, https://doi.org/10.2337/dci22-0043.
[3] H. Deng, B. Li, Q. Shen, C. Zhang, L. Kuang, R. Chen, G. Li, et al., Mechanisms of diabetic foot ulceration: a review, J. Diabetes 15 (4) (2023) 299–312, https://doi.org/10.1111/1753-0407.13372.
[4] J.L. Burgess, W.A. Wyant, B. Abdo Abujamra, R.S. Kirsner, I. Jozic, Diabetic wound-healing science, Medicina 57 (10) (2021) 1072, https://doi.org/10.3390/medicina57101072.
[5] O.A. Oyebode, S.W. Jere, N.N. Houreld, Current therapeutic modalities for the management of chronic diabetic wounds of the foot, J. Diabetes Res. 2023 (1) (2023) 1359537, https://doi.org/10.1155/2023/1359537.
[6] H. Huang, R. Xin, X. Li, X. Zhang, Z. Chen, Q. Zhu, L. Bao, Physical therapy in diabetic foot ulcer: research progress and clinical application, Int. Wound J. 20 (8) (2023) 3417–3434, https://doi.org/10.1111/iwj.14196.
[7] E.M. Tottoli, R. Dorati, I. Genta, E. Chiesa, S. Pisani, B. Conti, Skin wound healing process and new emerging technologies for skin wound care and regeneration, Pharmaceutics 12 (8) (2020) 735, https://doi.org/10.3390/pharmaceutics12080735.
[8] P. Kolimi, S. Narala, D. Nyavanandi, A.A.A. Youssef, N. Dudhipala, Innovative treatment strategies to accelerate wound healing: trajectory and recent advancements, Cells 11 (15) (2022) 2439, https://doi.org/10.3390/cells11152439.
[9] Q. Perrier, C. Moro, S. Lablanche, Diabetes in spotlight: current knowledge and perspectives of photobiomodulation utilization, Front. Endocrinol. 15 (2024) 1303638, https://doi.org/10.3389/fendo.2024.1303638.
[10] T.I. Karu, Multiple roles of cytochrome c oxidase in mam-malian cells under action of red and IR-A radiation, IUBMB Life 62 (2010) 607–610, https://doi.org/10.1002/iub.359.
[11] C. Dompe, L. Moncrieff, J. Matys, K. Grzech-Leśniak, I. Kocherova, A. Bryja, M. Dyszkiewicz-Konwińska, Photobiomodulation—underlying mechanism and clinical applications, J. Clin. Med. 9 (6) (2020) 1724, https://doi.org/10.3390/jcm9061724.
[12] O. Oyebode, N.N. Houreld, H. Abrahamse, Photobiomodulation in diabetic wound healing: a review of red and near-infrared wavelength applications, Cell Biochem. Funct. 39 (5) (2021) 596–612, https://doi.org/10.1002/cbf.3629.
[13] T.S. Leyane, S.W. Jere, N.N. Houreld, Cellular signalling and photobiomodulation in chronic wound repair, Int. J. Mol. Sci. 22 (20) (2021) 11223, https://doi.org/10.3390/ijms222011223.
[14] K. Wang, H. Zhao, X. Zhao, X. Zhang, W. Zhang, Y. Cheng, J. Ge, Photobiomodulation for diabetes and its complications: a review of general presentation, mechanisms and efficacy, Ann. Med. 56 (1) (2024) 2433684, https://doi.org/10.1080/07853890.2024.2433684.
[15] T.Y. Chung, P.V. Peplow, G.D. Baxter, Laser photobiostimulation of wound healing: defining a dose response for splinted wounds in diabetic mice, Lasers Surg. Med. 42 (9) (2010) 816–824, https://doi.org/10.1002/lsm.20981.
[16] N.R. Santos, J.N. dos Santos, J.A. dos Reis Jr, P.C. Oliveira, A.P.C. de Sousa, C. M. de Carvalho, A.L.B. Pinheiro, Influence of the use of laser phototherapy (λ660 or 790 nm) on the survival of cutaneous flaps on diabetic rats, Photomed. Laser Surg. 28 (4) (2010) 483–488, https://doi.org/10.1089/pho.2009.2500.
[17] F.A. Al-Watban, Laser therapy converts diabetic wound healing to normal healing, Photomed. Laser Surg. 27 (1) (2009) 127–135, https://doi.org/10.1089/pho.2008.2406.
[18] V.N. Hegde, V. Prabhu, S.B. Rao, S. Chandra, P. Kumar, K. Satyamoorthy, K. K. Mahato, Effect of laser dose and treatment schedule on excision wound healing in diabetic mice, Photochem. Photobiol. 87 (6) (2011) 1433–1441, https://doi.org/10.1111/j.1751-1097.2011.00991.x.
[19] M. Güngörmüş, U.K. Akyol, Effect of biostimulation on wound healing in diabetic rats, Photomed. Laser Surg. 27 (4) (2009) 607–610, https://doi.org/10.1089/pho.2008.2349.
[20] S.P. Swaminathan, M. Velayutham, S.M. Karthikeyan, M. Pakkiriappan, Low level red laser therapy using wavelength 635nm for diabetic foot ulcers: a prospective study, Int. Surg. J. 6 (2) (2019) 527, https://doi.org/10.18203/2349-2902.isj20190397.
[21] H.J. Choi, Z.A. Khan, A. Ansari, J. Choi, E.J. Kim, S.H. Han, H.J. Song, J.C. Jeong, Y. Hong, Comparison of wound healing effects of different micro-patterned hydrogels on the skin of secondary intention rat model, Gels 11 (4) (2025) 239, https://doi.org/10.3390/gels11040239.
[22] D.S. Masson-Meyers, T.A. Andrade, G.F. Caetano, F.R. Guimaraes, M.N. Leite, S. N. Leite, M.A.C. Frade, Experimental models and methods for cutaneous wound healing assessment, Int. J. Exp. Pathol. 101 (1–2) (2020) 21–37, https://doi.org/10.1111/iep.12346.
[23] B.S. Uysal, B. Sarıkaya, S.Ö. Akarca Dizakar, G. Take Kaplanoğlu, M. Gümüşderelioğlu, Investigation of healing strategies in a rat corneal opacity model with polychromatic light and stem cells injection, J. Photochem. Photobiol. B: Biol. 253 (2024) 112874, https://doi.org/10.1016/j.jphotobiol.2024.112874.
[24] S. Çıtak Demirez, T.S. Erkut, A. Sera Çakmak, Ö.A. Gürpınar, M. Gümüşderelioğlu, Therapeutic potential of near-infrared polychromatic light in hyperglycemic human cell models: toward improved diabetic wound healing, J. Photochem. Photobiol. B: Biol. 270 (2025) 113224, https://doi.org/10.1016/j.jphotobiol.2025.113224.
[25] A. Koyuncu, S. Koç, Ö.E. Akdere, A. Sera Çakmak, M. Gümüşderelioğlu, Investigation of the synergistic effect of platelet-rich plasma and polychromatic light on human dermal fibroblasts seeded chitosan/gelatin scaffolds for wound healing, J. Photochem. Photobiol. B: Biol. 232 (2022) 112476, https://doi.org/10.1016/j.jphotobiol.2022.112476.
[26] L. Ge, K. Wang, H. Lin, E. Tao, W. Xia, F. Wang, C. Mao, Y. Feng, Engineered exosomes derived from miR-132-overexpresssing adipose stem cells promoted diabetic wound healing and skin reconstruction, Front. Bioeng. Biotechnol. 11 (2023) 1129538, https://doi.org/10.3389/fbioe.2023.1129538.
[27] J. Huang, Q. Deng, L.L. Tsang, G. Chang, J. Guo, Y.C. Ruan, C.C. Wang, G. Li, H. F. Chan, X. Zhang, X. Jiang, Mesenchymal stem cells from perinatal tissues promote diabetic wound healing via PI3K/AKT activation, Stem Cell Res. Ther. 16 (1) (2025) 59, https://doi.org/10.1186/s13287-025-04141-8.
[28] L.S. Angelo, R. Kurzrock, Vascular endothelial growth factor and its relationship to inflammatory mediators, Clin. Cancer Res. 13 (10) (2007) 2825–2830, https://doi.org/10.1158/1078-0432.CCR-06-2416.
[29] H. Zhao, T. Ji, T. Sun, H. Liu, Y. Liu, D. Chen, Y. Gu, Comparative study on photobiomodulation between 630 nm and 810 nm LED in diabetic wound healing both in vitro and in vivo, J. Innov. Opt. Health Sci. 15 (02) (2022) 2250010, https://doi.org/10.1142/S1793545822500109.
[30] J.C. Tatmatsu-Rocha, C.R. Tim, L. Avo, R. Bernardes-Filho, P. Brassolatti, H. W. Kido, N.A. Parizotto, Mitochondrial dynamics (fission and fusion) and collagen production in a rat model of diabetic wound healing treated by photobiomodulation: comparison of 904 nm laser and 850 nm light-emitting diode (LED), J. Photochem. Photobiol. B: Biol. 187 (2018) 41–47, https://doi.org/10.1016/j.jphotobiol.2018.07.032.
[31] A.N. Otterço, A.L. Andrade, P. Brassolatti, K.N.Z. Pinto, H.S.S. Araújo, N. A. Parizotto, Photobiomodulation mechanisms in the kinetics of the wound healing process in rats, J. Photochem. Photobiol. B: Biol. 183 (2018) 22–29, https://doi.org/10.1016/j.jphotobiol.2018.04.010.
[32] G. Zhang, L. Yi, C. Wang, P. Yang, J. Zhang, J. Wang, Y. Liu, Photobiomodulation promotes angiogenesis in wound healing through stimulating the nuclear translocation of VEGFR2 and STAT3, J. Photochem. Photobiol. B: Biol. 237 (2022) 112573, https://doi.org/10.1016/j.jphotobiol.2022.112573.
[33] L.M. Wise, G.S. Stuart, N.C. Real, S.B. Fleming, A.A. Mercer, VEGF receptor-2 activation mediated by VEGF-E limits scar tissue formation following cutaneous injury, Adv. Wound Care 7 (8) (2018) 283–297, https://doi.org/10.1089/wound.2016.0721.
[34] R.W. Gilbert, M.K. Vickaryous, A.M. Viloria-Petit, Signalling by transforming growth factor beta isoforms in wound healing and tissue regeneration, J. Dev. Biol. 4 (2) (2016) 21, https://doi.org/10.3390/jdb4020021.
[35] R.P. Zaccaron, L. de Roch Casagrande, L.M. Venturini, J.V.S. Bittencourt, C. da Costa, E. de Pieri, P.C.L. Silveira, IL-1β antagonist receptor peptide associated with photobiomodulation accelerates diabetic wound tissue repair, Inflammation 47 (4) (2024) 1262–1277, https://doi.org/10.1007/s10753-024-01974-y.
[36] R. Fekrazad, A. Sarrafzadeh, K.A. Kalhori, I. Khan, P.R. Arany, A. Giubellino, Improved wound remodeling correlates with modulated TGF-beta expression in skin diabetic wounds following combined red and infrared photobiomodulation treatments, Photochem. Photobiol. 94 (4) (2018) 775–779, https://doi.org/10.1111/php.12914.
[37] Y. Dang, B. Liu, L. Liu, X. Ye, X. Bi, Y. Zhang, J. Gu, The 800-nm diode laser irradiation induces skin collagen synthesis by stimulating TGF-β/Smad signaling pathway, Lasers Med. Sci. 26 (2011) 837–843, https://doi.org/10.1007/s10103-011-0985-z.
[38] O.A. Oyebode, N.N. Houreld, Photobiomodulation at 830 nm stimulates migration, survival and proliferation of fibroblast cells, Diabetes Metab. Syndr. Obes. 21 (2022) 2885–2900, https://doi.org/10.2147/DMSO.S374649.
[39] H. Ramirez, S.B. Patel, I. Pastar, The role of TGFβ signaling in wound epithelialization, Adv. Wound Care 3 (7) (2014) 482–491, https://doi.org/10.1089/wound.2013.0466.

[40] B.C. Kim, H.T. Kim, S.H. Park, J.S. Cha, T. Yufit, S.J. Kim, V. Falanga, Fibroblasts from chronic wounds show altered TGF-β-signaling and decreased TGF-β type II receptor expression, J. Cell. Physiol. 195 (3) (2003) 331–336, https://doi.org/10.1002/jcp.10301.

[41] M. Rahmannia, A. Amini, S. Chien, M. Bayat, Impact of photobiomodulation on macrophages and their polarization during diabetic wound healing: a systematic review, Lasers Med. Sci. 37 (7) (2022) 2805–2815, https://doi.org/10.1007/s10103-022-03581-5.

[42] R. Ebrahimpour-Malekshah, A. Amini, A. Mostafavinia, H. Ahmadi, F. Zare, S. Safaju, M. Bayat, The stereological, immunohistological, and gene expression studies in an infected ischemic wound in diabetic rats treated by human adipose-derived stem cells and photobiomodulation, Arch. Dermatol. Res. 315 (6) (2023) 1717–1734, https://doi.org/10.1007/s00403-023-02563-z.

[43] D. Vatandoust, H. Ahmadi, A. Amini, A. Mostafavinia, F.F. Fathabady, A. Moradi, M. Bayat, Photobiomodulation preconditioned diabetic adipose derived stem cells with additional photobiomodulation: an additive approach for enhanced wound healing in diabetic rats with a delayed healing wound, Lasers Med. Sci. 39 (1) (2024) 86, https://doi.org/10.1007/s10103-024-04034-x.

[44] T.N. Mgwenya, H. Abrahamse, N.N. Houreld, Modulatory effects of 830 nm on diabetic wounded fibroblast cells: an In vitro study on inflammatory cytokines, photobiomodulation, Photomed. Laser Surg. 42 (11) (2024) 676–692, https://doi.org/10.1089/photob.2024.0041.

[45] J. Hu, X. Dong, Y. Lv, D. Hu, D. Fei, H. Dong, H. Yin, Biphasic photobiomodulation of inflammation in mouse models of common wounds, infected wounds, and diabetic wounds, J. Photochem. Photobiol. B: Biol. 252 (2024) 112868, https://doi.org/10.1016/j.jphotobiol.2024.112868.

[46] P.D.T.C.D. Carvalho, N. Mazzer, F.A.D. Reis, A.C.G. Belchior, I.S. Silva, Analysis of the influence of low-power HeNe laser on the healing of skin wounds in diabetic and non-diabetic rats, Acta Cirúrgica Brasileira 21 (2006) 177–183, https://doi.org/10.1590/s0102-86502006000300010.

[47] I.B. do Valle, P.H.D.M. Prazeres, R.A. Mesquita, T.A. Silva, H.M. de Castro Oliveira, P.R. Castro, I.M.A. Diniz, Photobiomodulation drives pericyte mobilization towards skin regeneration, Sci. Rep. 10 (1) (2020) 19257, https://doi.org/10.1038/s41598-020-76243-7.

[48] G. Kesava Reddy, Comparison of the photostimulatory effects of visible He-Ne and infrared Ga-As lasers on healing impaired diabetic rat wounds, Lasers Surg. Med. Offic. J. Am. Soc. Laser Med. Surg. 33 (5) (2003) 344–351, https://doi.org/10.1002/lsm.10227.

[49] G.A. Maiya, P. Kumar, L. Rao, Effect of low intensity helium-neon (He-Ne) laser irradiation on diabetic wound healing dynamics, Photomed. Laser Therapy 23 (2) (2005) 187–190, https://doi.org/10.1089/pho.2005.23.187.

[50] R. Zein, W. Selting, M.R. Hamblin, Review of light parameters and photobiomodulation efficacy: dive into complexity, J. Biomed. Opt. 23 (12) (2018) 1–17, https://doi.org/10.1117/1.JBO.23.12.120901.

[51] N. Houreld, H. Abrahamse, Irradiation with a 632.8 nm helium-neon laser with 5 J/cm2 stimulates proliferation and expression of interleukin-6 in diabetic wounded fibroblast cells, Diabetes Technol. Ther. 9 (5) (2007) 451–459, https://doi.org/10.1089/dia.2007.0203.

[52] T.N. Mgwenya, H. Abrahamse, N.N. Houreld, Photobiomodulation studies on diabetic wound healing: an insight into the inflammatory pathway in diabetic wound healing, Wound Repair Regen. 33 (1) (2025) e13239, https://doi.org/10.1111/wrr.13239.